Available online at www.sciencedirect.com
ScienceDirect
Trans. Nonferrous Met. Soc. China 32(2022) 1096−1104
Transactions of Nonferrous Metals Society of China
www.tnmsc.cn

Effect of strain rate on microstructure and mechanical properties of spray-formed Al−Cu−Mg alloy

Tong SHEN[1], Cai-he FAN[1,2], Ze-yi HU[1], Qin WU[1], Yu-meng NI[1], Yu-zhou CHEN[3]

1. College of Materials and Advanced-Manufacturing, Hunan University of Technology, Zhuzhou 412007, China;
2. Anhui Jianye Science and Technology Co., Ltd., Huaibei 235000, China;
3. Hunan Zhirong Science and Technology Co., Ltd., Zhuzhou 412000, China

Received 20 August 2021; accepted 17 February 2022

Abstract: Transmission electron microscopy (TEM), X-ray diffraction (XRD), electron backscattered diffraction (EBSD), and tensile tests were used to study the effects of strain rates (0.1, 1 and 9.1 s^{-1}) on the microstructure and mechanical properties of spray-formed Al−Cu−Mg alloys during large-strain rolling at 420 °C. Results show that during hot rolling, the proportion of high-angle grain boundaries (HAGBs) and the degree of dynamic recrystallization (DRX) initially increase and then decrease, whereas the average grain size and dislocation density show the opposite trend with the increase of the strain rate. In addition, the number of S' phases in the matrix decreases, and the grain boundary precipitates (GBPs) become coarser and more discontinuous as the strain rate increases. When the strain rate increases from 0.1 to 9.1 s^{-1}, the tensile strength of the alloy decreases from 492.45 to 427.63 MPa, whereas the elongation initially increases from 12.1% to 21.8% and then decreases to 17.7%.

Key words: spray forming; Al−Cu−Mg alloy; strain rate; microstructure; mechanical properties

1 Introduction

The Al−Cu−Mg alloys have been widely used in aerospace and military fields because of their high strength and good processability and formability [1,2]. As an important parameter in the processing of Al−Cu−Mg alloy, the strain rate has been widely studied. ZHANG et al [3] studied the effect of strain rate on the redissolution rate of precipitated phase in Al−Cu alloy at low temperature during severe plastic deformation, and found that the higher the strain rate is, the smaller the deformation amount required for redissolution of precipitated phases is. WANG et al [4] studied the influence of strain rate and deformation temperature on the mechanical properties of Al−Cu−Mg alloy after equal channel angular pressing. Under the conditions of higher strain rates and lower deformation temperatures, the flow stress and strain hardening increase significantly. GAO et al [5] reported that a high strain rate can reduce the transition temperature of the θ' phase in 2519 aluminum alloy. Different strain rates will induce complex strain rate effects in the aluminum alloys. WANG et al [6] found that the flow stress of 2024 aluminum alloy at a certain temperature is proportional to the strain rate. In addition, ZHANG [7] carried out tensile and compression tests on 2024 aluminum alloy at different strain rates (10^{-4}–10^{3} s^{-1}). The experimental results show that the effect of strain rate on yield stress is not evident, whereas the toughness decreases and the brittleness increases at higher strain rate.

In this study, we aims to improve the production efficiency and subsequent performance in aluminum alloy cartridge cases. Understanding the effect of strain rate on the microstructure and

Corresponding author: Cai-he FAN, Tel: +86-731-22183432, E-mail: 369581813@qq.com
DOI: 10.1016/S1003-6326(22)65879-5

mechanical properties of the spray-formed Al−Cu−Mg alloy is of great significance to further improve subsequent performance of aluminum alloy cartridge cases. Previous studies were primarily focused on Al−Cu−Mg alloys prepared by conventional processes, whereas the effect of strain rate on the spray-formed Al−Cu−Mg alloy is rarely reported. Based on rapid solidification of fine-grained Al−Cu−Mg alloy billet prepared by spray forming, the microstructure evolution, mechanical properties, and strengthening and toughening mechanism of Al−Cu−Mg alloy under different strain rates were studied to guide subsequent heat treatment process.

2 Experimental

A rapidly-solidified fine-grained Al−Cu−Mg alloy cylindrical ingot was prepared on a self-developed SD380 large-scale injection molding apparatus. Table 1 gives the chemical composition of the Al−Cu−Mg alloy.

Table 1 Chemical composition of Al−Cu−Mg alloy (wt.%)

Cu	Mg	Mn	Si	Fe	Al
4.0	1.7	0.4	<0.05	<0.03	Bal.

The cylindrical ingot was extruded into a plate with a sectional size of 20 mm×10 mm using a 1250T extruder at 450 °C with an extrusion ratio of 15:1. The samples were pre-heated for 30 min at 420 °C, and then hot-rolled at different strain rates (0.1, 1 and 9.1 s^{-1}) with 4 passes. The total rolling reduction was 80%, and the specific rolling parameters are given in Table 2. The motor transmission ratio of the rolling machine is 31.5, and the maximum motor speed is 1500 r/min.

The microstructure evolution of the deformed sample was investigated by EBSD on the scanning electron microscope (SEM, FEI Quanta 2000). The EBSD samples were prepared by electro-polishing using a solution of 80% C_2H_5OH and 20% $HClO_4$ at 20 V for 30 s. The EBSD samples were detected by Aztec software, performing at the operating potential of 30 kV and tilting angle of 70° with 0.2 μm scanning steps. The microstructure of the sample was analyzed using a JEM−F200 transmission electron microscope (TEM). The sample was mechanically pre-thinned to approximately 80 μm, and then twin-jet electro-polished with a solution of nitric acid and methanol (volume ratio of 1:3) at the temperature lower than −25 °C. The phase identification was done by a D/max 2500 18 kW target X-ray diffraction. The tensile test was performed on the American Instron 3369 mechanical testing machine with the tensile rate of 1 mm/min.

Table 2 Technological parameters of rolling

Rolling pass	Rolling reduction/mm	Motor speed/(r·min^{-1})	Strain rate/s^{-1}
1	2	1470, 161, 16	9.1, 1, 0.1
2	2	1171, 129, 13	9.1, 1, 0.1
3	2	878, 96, 10	9.1, 1, 0.1
4	2	585, 64, 6	9.1, 1, 0.1

3 Results

3.1 XRD pattern

The XRD patterns of the hot-rolled Al−Cu−Mg alloy samples under different strain rates are shown in Fig. 1. It can be seen that, the main precipitates of the Al−Cu−Mg alloy sample are α phase (Al) and S' phase (Al_2CuMg). The highest diffraction peak intensity of the S' phase is obtained at 0.1 s^{-1}. With the increase of strain rate, the diffraction peak intensity of the S' phase decreases gradually. By quantitatively analyzing and calculating the S' phase, the volume fractions of the S' phase at the strain rates of 0.1, 1 and 9.1 s^{-1} are 1.4%, 1.1% and 0.4%, respectively. The volume fraction of the S' phase decreases with the increase of strain rate.

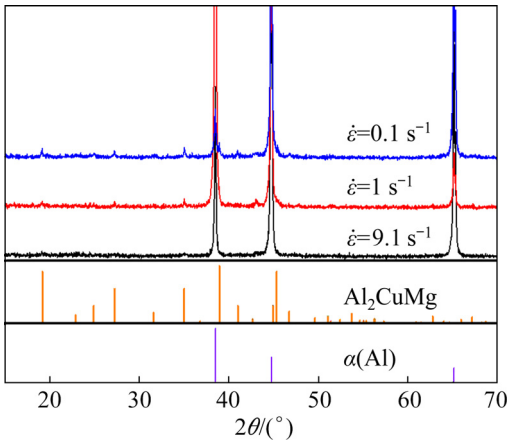

Fig. 1 XRD patterns of hot-rolled Al−Cu−Mg alloy samples under different strain rates

3.2 Microstructure

Figure 2 shows the inverse pole figures (IPFs), DRX grain size distributions and misorientation angle distributions of the hot-rolled Al−Cu−Mg alloy under different strain rates. The IPFs show that the grain orientation in the alloy is random and DRX occurs at different strain rates. When the strain rate increases from 0.1 to 1 s^{-1}, the degree of DRX increases; however, the degree decreases with the strain rate up to 9.1 s^{-1}. Based on DRX grain size distribution (Figs. 2(b, e, h), the average grain sizes at 0.1, 1 and 9.1 s^{-1} are 8.9, 5.8 and 11.7 μm, respectively. With the increase of the strain rate, the DRX grain size firstly decreases and then increases, and the grains are significantly refined at 1 s^{-1} (Fig. 2(e)). According to the misorientation angle distributions (Figs. 2(c, f, i), the proportion of HAGBs (>15°) initially increases from 72.3% to 81.2%, and then decreases to 63.8% with the increase of strain rate from 0.1 to 9.1 s^{-1}.

Figure 3 shows the Kernel average misorientation (KAM) figures of the hot-rolled Al−Cu−Mg alloy under different strain rates. The KAM maps are often used to reveal local misorientation, and the green lines in the maps can be approximately regarded as dislocations. After calculation, the dislocation densities in the alloy at strain rate of 0.1, 1 and 9.1 s^{-1} are 2.92×10^{14}, 2.78×10^{14} and 3.53×10^{14} m^{-2}, respectively. That is to say, the dislocation density slightly decreases

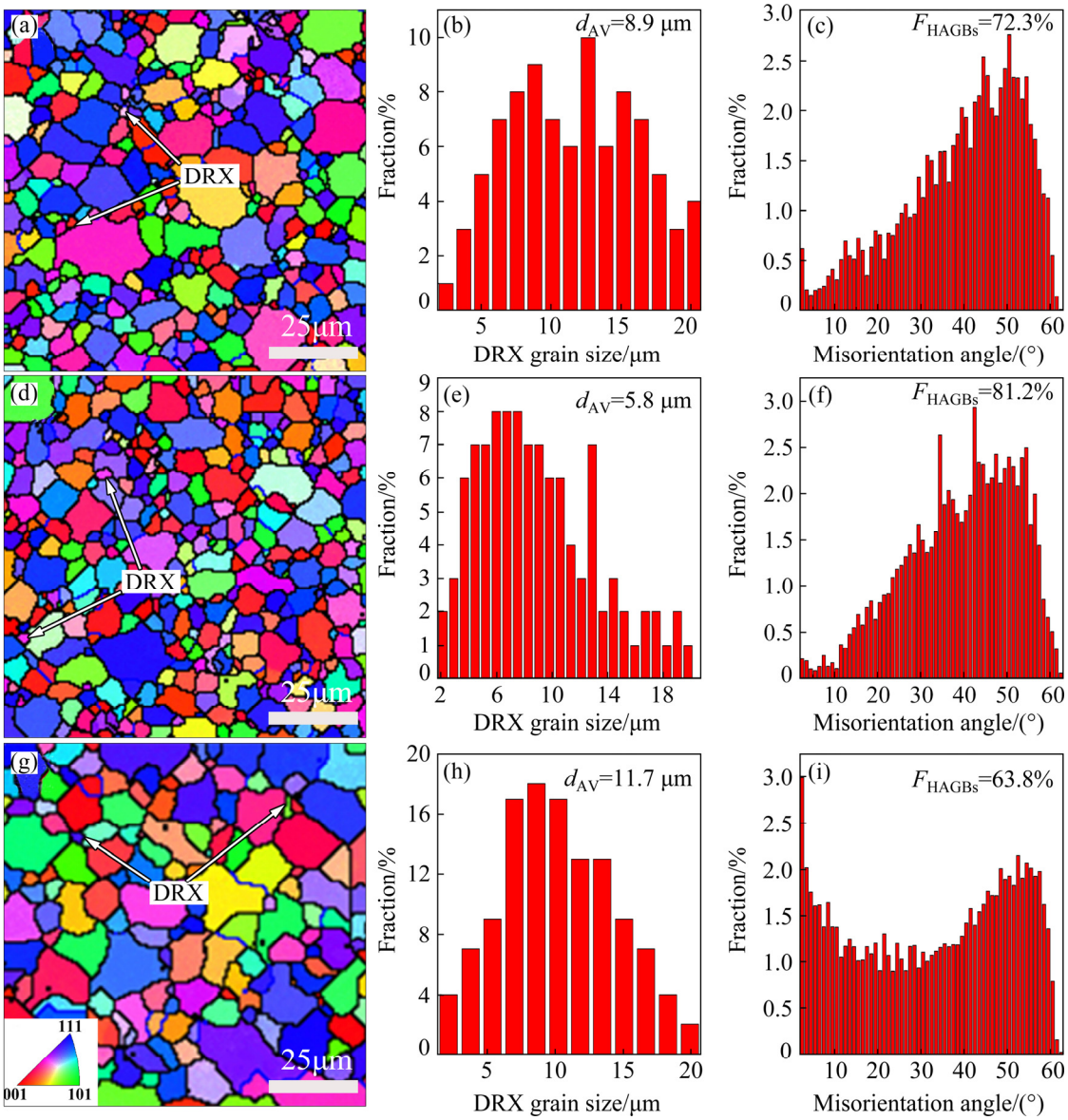

Fig. 2 IPFs (a, d, g), DRX grain size distributions (b, e, h) and misorientation angle distributions (c, f, i) of hot-rolled Al−Cu−Mg alloy under different strain rates: (a, b, c) $\dot{\varepsilon}$ =0.1 s^{-1}; (d, e, f) $\dot{\varepsilon}$ =1 s^{-1}; (g, h, i) $\dot{\varepsilon}$ =9.1 s^{-1}

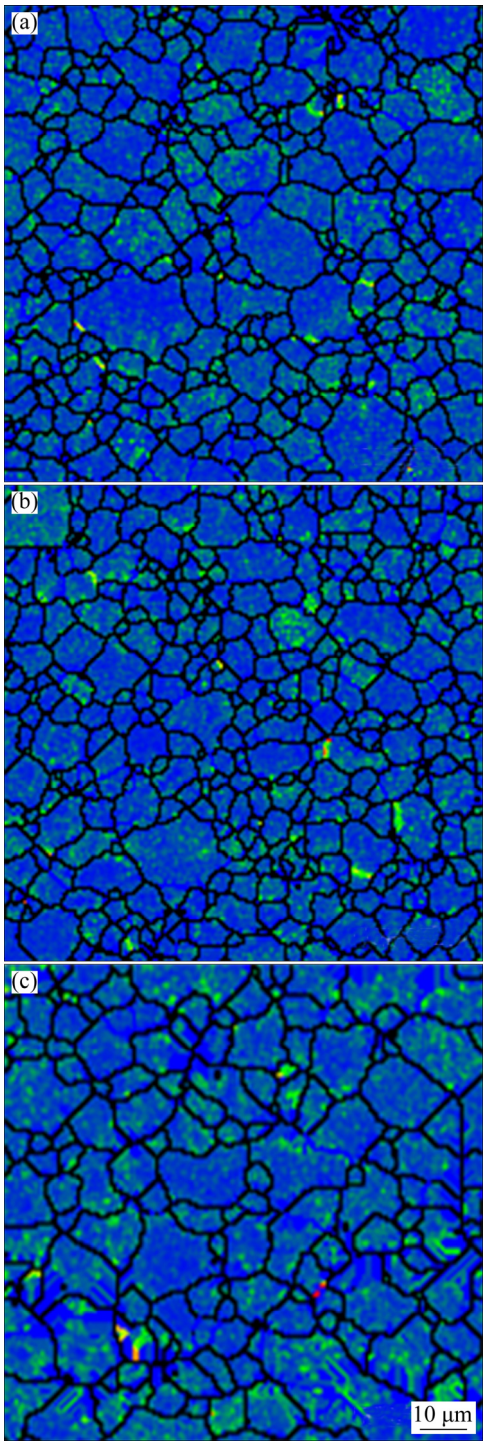

Fig. 3 KAM maps of hot-rolled Al−Cu−Mg alloy under different strain rates: (a) $\dot{\varepsilon}$ =0.1 s^{-1}; (b) $\dot{\varepsilon}$ =1 s^{-1}; (c) $\dot{\varepsilon}$ =9.1 s^{-1}

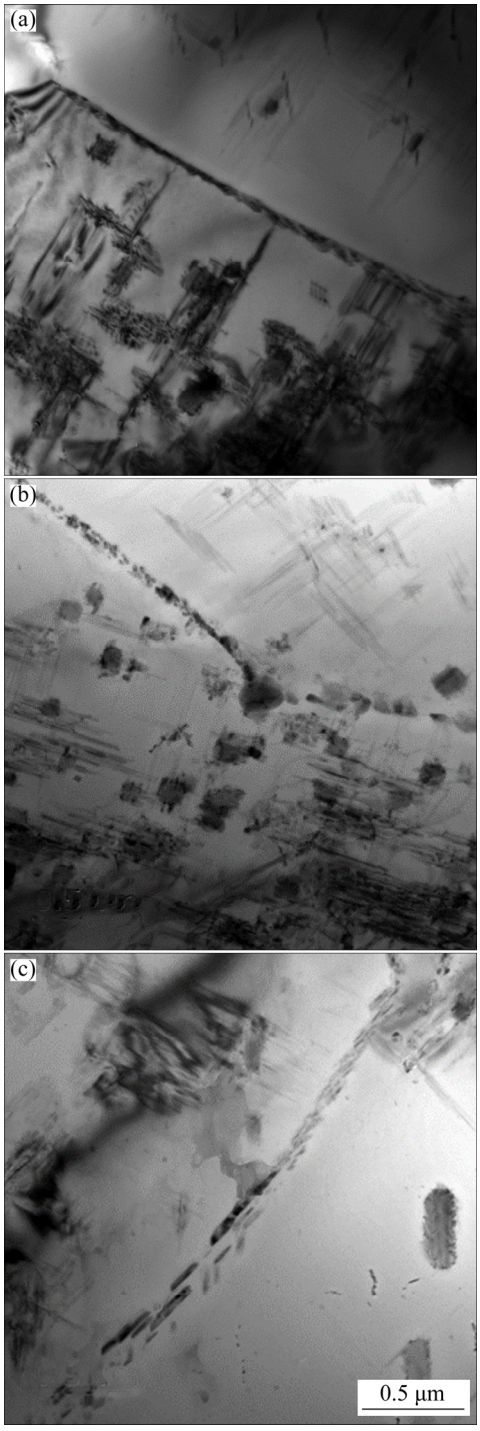

Fig. 4 TEM images of hot-rolled Al−Cu−Mg alloy under different strain rates: (a) $\dot{\varepsilon}$ =0.1 s^{-1}; (b) $\dot{\varepsilon}$ =1 s^{-1}; (c) $\dot{\varepsilon}$ =9.1 s^{-1}

with the increase of strain rate from 0.1 to 1 s^{-1} (Figs. 3(a, b)), and then increases as the strain rate increases up to 9.1 s^{-1} (Fig. 3(c)).

Figure 4 presents the TEM images of the hot-rolled Al−Cu−Mg alloy under the strain rate of 0.1, 1 and 9.1 s^{-1}. As shown in Fig. 4(a), the GBPs are continuously distributed in the alloy rolled at the strain rate of 0.1 s^{-1}. With the strain rate increasing to 1 s^{-1}, the GBPs are found to be more discontinuous, and the GBP size grows slightly (Fig. 4(b)). When being hot-rolled at the strain rate of 9.1 s^{-1}, the GBPs show evident coarsening and discontinuity.

3.3 Tensile properties

The tensile curves of the hot-rolled Al−Cu−Mg alloy samples under different strain rates are shown in Fig. 5, and the values of tensile strength, yield strength and elongation are given in Table 3. It can be seen from Table 3 that the tensile strength and yield strength decrease gradually, while the elongation firstly increases and then decreases with the increase of strain rate. When the strain rate is 0.1 s^{-1}, the sample has the highest tensile strength and yield strength, which are 492.45 and 361.52 MPa, respectively. The highest elongation of 21.8% is obtained at the strain rate of 1 s^{-1}.

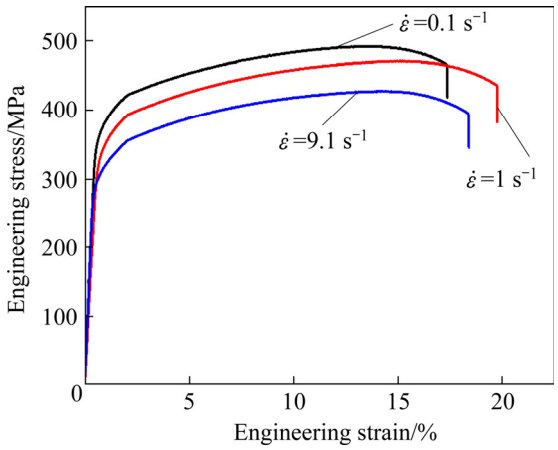

Fig. 5 Tensile curves of hot-rolled Al−Cu−Mg alloy samples under different strain rates

Table 3 Mechanical properties of hot-rolled Al−Cu−Mg alloy under different strain rates

Strain rate/s^{-1}	Tensile strength/MPa	Yield strength/MPa	Elongation/%
0.1	492.45±5	361.52±5	12.1±1
1	471±5	336.31±5	21.8±1
9.1	427.63±5	297.8±5	17.7±1

4 Discussion

4.1 Evolution mechanism of recrystallization and dislocation at different strain rates

As shown in Fig. 2, the size of DRX grains initially decreases and then increases with the increase of strain rate, and the proportion of HAGBs shows the opposite trend. Recrystallization is driven by the strain energy stored in the alloy during deformation [8,9]. When the strain rate is 0.1 s^{-1}, the atoms in alloy have enough time to fully diffuse, thereby producing enough strain energy to stimulate the nucleation of DRX. In addition, the deformation time of the sample is long enough for the grain boundary migration at the low strain rate of 0.1 s^{-1}, resulting in enough time for grain growth. As the alloy continues to deform, not only the original grains but also the new DRX grains undergo deformation, and the low-angle grain boundaries (LAGBs) continue to form in the alloy [10]. With the strain rate increasing to 1 s^{-1}, the energy of alloy system increases, and more of them can be used for subcrystalline growth and new grain nucleation. Thus, more new grains with HAGBs are formed. Moreover, the growth time of DRX grains is limited because of the increased strain rate, resulting in refined grains. When the strain rate increases to 9.1 s^{-1}, the DRX grain size and the proportion of LAGBs increase significantly, which may be due to the shortened deformation time and temperature rise at a high strain rate [11]. Although the driving force of recovery and recrystallization is certainly high at a high strain rate, the shortened deformation time limits the degree of dynamic recovery and recrystallization [12]. As shown in Fig. 2(g), a few DRX grains with small sizes are observed, while the overall grain refinement is not obvious. The driving force of grain boundary migration is the distortion energy of the deformed metal [13]. At a higher strain rate, the distortion energy increases significantly, and the grain boundary migration ability is enhanced with the increase of temperature, thereby increasing the grain size.

The hot deformation process is overlapped by two opposite processes: recrystallization softening process and work hardening. DRX grains undergo work hardening during growing, forming dislocation density gradients in grains. According to the calculation results shown in Fig. 3, the dislocation density in the alloy firstly decreases and then increases with the increase of strain rate. In the recovery stage of hot deformation, the reduction of dislocation density is limited. Moreover, the dislocation density will decrease significantly only in the recrystallization stage. Compared with the alloy rolled at the strain rate of 0.1 s^{-1}, the degree of DRX increases significantly, and the rearrangement of dislocation becomes more sufficient at 1 s^{-1}, resulting in the decreases in dislocation density. When the strain rate increases to 9.1 s^{-1}, the

opportunities of adjacent grain orientation against deformation increase, and the number of dislocations in the grain increases greatly. At the same time, the increase of strain rate weakens dislocation rearrangement or annihilation, and hinders DRX, leading to a significant increase in dislocation density in the alloy.

4.2 Evolution mechanism of *S′* phase at different strain rates

The mass ratio of Cu/Mg in the experimental sample is 2.35. According to the literatures [14,15], *S′* phase is the main strengthening phase of the Al−Cu−Mg alloy with a low Cu/Mg ratio. As shown in Fig. 6(a), the *S′* phase is distorted and broken under the action of large stress, and the fracture of *S′* phase improves the interfacial distortion energy between the *S′* phase and the aluminum matrix. In addition, resolved steps and necking are detected in the *S′* phase (Figs. 6(b, c)), which promotes the redissolution of the *S′* phase, and finally reduces the size and volume fraction of the *S′* phase. According to the calculations, the increase of strain rate leads to a significant reduction in the number of the *S′* phases. During large-strain hot-rolling, the effect of temperature rise becomes evident with the increase of strain rate. PINHEIRO et al [16] showed that the adiabatic temperature rise of deformation can be ignored at a low strain rate (<1 s^{-1}). Therefore, the temperature rise in the alloy hot-rolled at the strain rate of 0.1 s^{-1} can be ignored. However, the temperature rise increases the maximum solid solubility of Al−Cu−Mg alloy and prevents the precipitation of *S′* phase at a higher strain rate (≥1 s^{-1}). Moreover, a higher strain rate shortens the deformation time and inhibits the nucleation and growth of the *S′* phase. Therefore, redissolution of the *S′* phase combined with precipitating obstruction reduces the number of the *S′* phases in alloy hot-rolled at a higher strain rate.

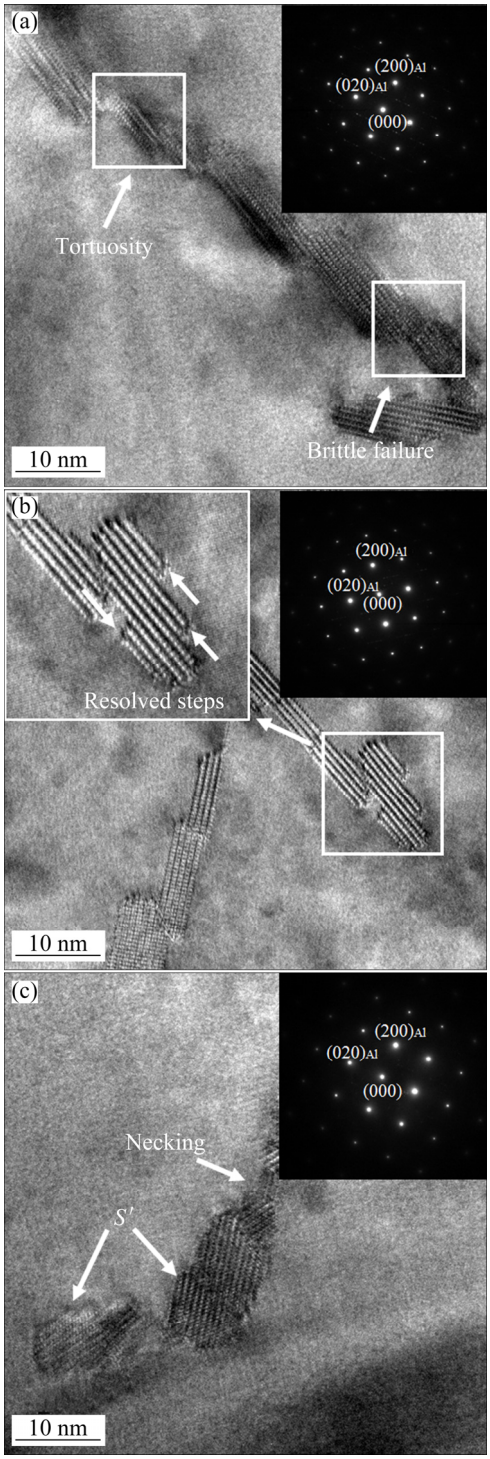

Fig. 6 TEM images of *S′* phase in hot-rolled Al−Cu−Mg alloy: (a) Distortion and brittle fracture of *S′* phase; (b) Resolved steps of *S′* phase; (c) Necking of *S′* phase

4.3 Effect of strain rate on strengthening and toughening mechanism of spray-formed Al−Cu−Mg alloys

Figure 5 shows that during rolling, the tensile strength and yield strength of the Al−Cu−Mg alloy decrease significantly with the increase of strain rate. The plastic deformation in the alloy is driven by dislocation slip, and the strengthening is realized by hindering the dislocation movement through precipitates, solute atoms, and grain boundaries. The yield strength of polycrystalline materials can be expressed as [17]

$$\sigma_{\text{total}} = \sigma_0 + \Delta\sigma_{\text{prec}} + \Delta\sigma_{\text{GB}} + \Delta\sigma_{\text{dis}} + \Delta\sigma_{\text{ss}} \quad (1)$$

where σ_0 is the yield strength of pure alloy (20 MPa); $\Delta\sigma_{prec}$, $\Delta\sigma_{GB}$, $\Delta\sigma_{dis}$ and $\Delta\sigma_{ss}$ represent the yield strength increments produced by the precipitation strengthening, the grain boundary strengthening, the dislocation strengthening and the solid solution strengthening, respectively.

The increment in precipitation strengthening can be estimated using Orowan mechanism [18]:

$$\Delta\sigma_{prec}=\sqrt{3}Gb/L \quad (2)$$

where L is the mean distance between precipitates, G (=27 GPa) is the shear modulus, and b is the magnitude of Burgers vector. Based on the measurements of more than 120 particles in 9 TEM micrographs, the average distance (L) at strain rates of 0.1, 1 and 10 s^{-1} are 91, 115 and 159 nm, respectively. Therefore, the increment in the yield strength is 146, 116, and 84 MPa at strain rates of 0.1, 1 and 9.1 s^{-1}, respectively.

The value of $\Delta\sigma_{GB}$ generated by grain boundary strengthening can be described by the Hall−Petch equation [19]:

$$\Delta\sigma_{GB}=kd^{-1/2} \quad (3)$$

where k is the Hall−Petch coefficient for Al−4Cu alloy (0.1 MPa·$m^{1/2}$), and d is the grain size. At strain rates of 0.1, 1 and 9.1 s^{-1}, the values of $\Delta\sigma_{GB}$ are 33, 41 and 28 MPa, respectively.

The relationship between $\Delta\sigma_{dis}$ and dislocation density (ρ) is shown as follows [20]:

$$\Delta\sigma_{dis}=\alpha MGb\rho^{1/2} \quad (4)$$

where α (=0.3) is a constant, b=2.86×10^{-10} m and M (=3) is the Taylor factor. At strain rates of 0.1, 1 and 9.1 s^{-1}, the values of $\Delta\sigma_{dis}$ are 119, 116 and 131 MPa, respectively.

The value of $\Delta\sigma_{ss}$ related to the concentration of solute can be calculated by the following equation [21]:

$$\Delta\sigma_{ss}=2AC_0^{2/3} \quad (5)$$

where A (=12.43) is a constant and C_0 is the mass fraction of solute. According to the results in Fig. 1, the mass fractions of the S' phase at strain rates of 0.1, 1 and 9.1 s^{-1} is 3.23%, 2.93% and 2.24%, respectively. By assuming the remaining Cu and Mg atoms are completely dissolved in the Al matrix, the values of C_0 at strain rates of 0.1, 1 and 9.1 s^{-1} are 2.47, 2.77 and 3.46 wt.%, respectively. The yield strength increments by solid solution strengthening are approximately 45, 49 and 56 MPa when the strain rates are 0.1, 1 and 9.1 s^{-1}, respectively.

As shown in Fig. 7, the theoretical yield strengths of the Al−Cu−Mg alloy under different strain rates are obtained, which are compared with the experimental values. The theoretical values of σ_{total} are close to the experimental ones.

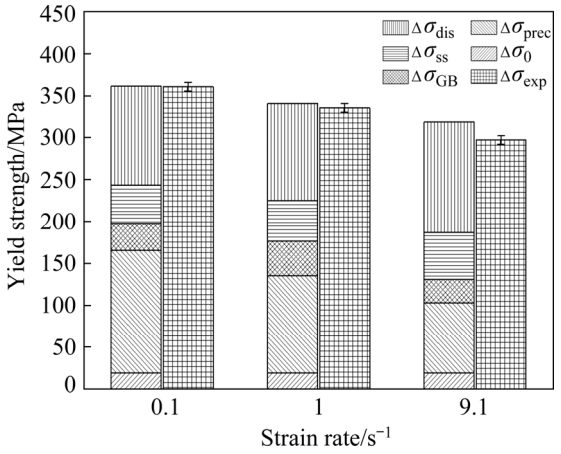

Fig. 7 Comparison of theoretical and experimental yield strength values

It can be seen from Figs. 1 and 7 that the mass fraction of the S' phase is the largest in the alloy at the strain rate of 0.1 s^{-1}, and the main strengthening mode of the alloy is precipitation strengthening. When the strain rate is 1 s^{-1}, the precipitation strengthening effect is weakened, while the grains are refined due to the more sufficient DRX that occurs in the sample, and the fine grain strengthening contributes part of the strength in this case. When the strain rate is 9.1 s^{-1}, the amount of S' phase is obviously reduced, and a lot of broken dispersed phases are detected in the matrix. The interaction between S' phase and dislocation could reduce the size of the S' phase. As the size is less than a critical value, the broken and dispersed S' phase would dissolve and disappear [22]. Thus, the contribution of precipitation strengthening to the strength of the material is weakened. In addition, the grain size increases at the strain rate of 9.1 s^{-1}, resulting in a weakened fine grain strengthening effect. As shown in Figs. 3 and 7, the dislocation density in the sample hot-rolled at 9.1 s^{-1} is the highest. Above all, dislocation strengthening is the main strengthening mode at the strain rate of 9.1 s^{-1}.

As shown in Fig. 4, when the strain rate is

0.1 s^{-1}, the GBPs are densely distributed, which increases the stress concentration and accelerates the crack growth, resulting in poor plasticity. When the strain rate is 1 s^{-1}, the alloy exhibits the best plasticity, resulting from the combined action of GBPs and temperature rise. Coarsening GBPs reduce the plasticity of the alloy, while the temperature rise has a more significant effect on the plasticity at the strain rate of 1 s^{-1}. The temperature rise leads to the decrease of lattice resistance to dislocation movement and a more uniform dislocation distribution [23]. During high-temperature deformation, multiple slip systems can start at the same time, and can smoothly bypass the dislocation obstacles, which promotes the uniform deformation of the material, thereby making up for the loss of plasticity caused by coarsening GBPs. When the strain rate increases to 9.1 s^{-1}, the diffusion of solute atoms accelerates, and GBPs significantly become coarser and more discontinuous, resulting in a decrease in plasticity compared with the alloy hot rolled at the strain rate of 1 s^{-1}.

In summary, with the increase of strain rates during large-strain hot-rolling, the strength of spray-formed Al−Cu−Mg alloys decreases, while the plasticity initially increases and then decreases because of the combined effects of precipitates, dislocations and recrystallization.

5 Conclusions

(1) During large-strain hot-rolling, the tensile strength and yield strength of the spray-formed Al−Cu−Mg alloy decrease continuously with the strain rate increasing from 0.1 to 9.1 s^{-1} at 420 °C. The elongation initially increases and then decreases with the increase of strain rate.

(2) As the strain rate increases, the degree of DRX firstly increases and then decreases, the average grain size shows the opposite trend, and the GBPs become coarser and more discontinuous. The larger the HAGBs proportion, the higher the DRX degree and the finer the grain size are obtained in the alloy hot-rolled at the strain rate of 1 s^{-1}.

(3) With the increase of strain rate, the dislocation density firstly decreases and then increases, and the density of the S' phase decreases. Precipitation strengthening is the main strengthening mode at the strain rate of 0.1 s^{-1}, whereas dislocation strengthening dominates at the strain rate of 9.1 s^{-1}.

Acknowledgments

This work was financially supported by the Major Special Projects in Anhui Province, China (No. 202003c08020005), and the Key Projects in Hunan Province, China (No. 2020GK2045).

References

[1] WANG Zhu-tang, TIAN Rong-zhang. User Manual for Al Alloys and Processing Version [M]. 3rd ed. Changsha: Central South University Press, 2007. (in Chinese)

[2] WILLIAMS J C, STARKE J E. Progress in structural materials for aerospace systems [J]. Acta Materialia, 2003, 51(19): 5775−5799.

[3] ZHANG Zi-zhao, XU Xiao-chang, LIU Zhi-yi, WU Chun. Effect of strain rate on redissolution rate of precipitated phase at low temperature in severely plastically deformed Al−Cu alloy [J]. Heat Treatment, 2010, 25(2): 15−18. (in Chinese)

[4] WANG Lei, DU Meng, TAN Hao, XI Yun-tao, ZHONG Yu-jie, WANG Shi-qing. Influence of strain rate and temperature on mechanical properties of 2A12 aluminum alloys after equal channel angular pressing [J]. Transactions of Materials and Heat Treatment, 2018, 39(5): 126−133, 140.

[5] GAO Zhi-guo, ZHANG Xin-ming, CHEN Ming-an. Influence of strain rate on the precipitate microstructure in impacted aluminum alloy [J]. Scripta Materialia, 2008, 59(9): 983−986.

[6] WANG Jin-peng, ZENG Pan, LEI Li-ping. Dynamic plastic experiments and constitutive model of 2024 aluminum under high temperature and high strain rate [J]. Journal of Plasticity Engineering, 2008, 15(3): 101−104. (in Chinese)

[7] ZHANG Zheng-li. Testing of dynamic mechanical property of several aluminum alloy materials [J]. Journal of Civil Aviation University of China, 2014, 32(1): 41−45. (in Chinese)

[8] SHI Zhao-Xia, YAN Xiao-feng, DUAN Chun-hua, ZHAO Ming-han. Effect of strain rate on hot deformation characteristics of GH690 superalloy [J]. Transactions of Nonferrous Metals Society of China, 2017, 27(3): 538−550.

[9] ZHANG Hong-bin, ZHANG Kai-feng, ZHOU Hai-ping, LU Zhen, ZHAO Chang-hong, YANG Xiao-li. Effect of strain rate on microstructure evolution of a nickel-based superalloy during hot deformation [J]. Materials & Design, 2015, 80: 51−62.

[10] YU Yong-ling. Principles of Metallography [M]. 2rd ed. Beijing: Metallurgical Industry Press, 2013. (in Chinese)

[11] LIAO Bin, WU Xiao-dong, YAN Chang-jian, LIU Zheng, JI Yan-li, GAO Ling-fei, HUANG Guang-jie, LIU Qing. Microstructure characterization of Al-cladded Al–Zn–Mg–Cu sheet in different hot deformation conditions [J]. Transactions of Nonferrous Metals Society of China, 2017, 27(8): 1689−1697.

[12] WU B, LI M Q, MA D W. The flow behavior and

constitutive equations in isothermal compression of 7050 aluminum alloy [J]. Materials Science and Engineering A, 2012, 542: 79−87.
[13] WANG W, BRISSET F, HELBERT A L, SOLAS D, MATHON M H, BAUDIN T. Influence of stored energy on twin formation during primary recrystallization [J]. Materials Science and Engineering A, 2014, 589: 112−118.
[14] ZHANG J, HUANG Y N, MAO C, PENG P. Structural, elastic and electronic properties of θ(Al_2Cu) and S(Al_2CuMg) strengthening precipitates in Al−Cu−Mg series alloys: First-principles calculations [J]. Solid State Communications, 2012, 152(23): 2100−2104.
[15] PUGH S F. Relations between the elastic moduli and the plastic properties of polycrystalline pure metals [J]. The London, Edinburgh, and Dublin Philosophical Magazine and Journal of Science, 1954, 45(367): 823−843.
[16] PINHEIRO I P, BARBOSA R, CETLIN P R. The relevance of dynamic recrystallization in the hot deformation of IF steel at high strain rates [J]. Materials Science and Engineering A, 2007, 457: 90−93.
[17] CHAKRABARTI D J, LAUGHLIN D E. The Cr−Cu (chromium−copper) system [J]. Bulletin of Alloy Phase Diagrams, 1984, 5(1): 59−68.
[18] HUSKINS E L, CAO B, RAMESH K T. Strengthening mechanisms in an Al−Mg alloy [J]. Materials Science and Engineering A, 2010, 527: 1292−1298.
[19] LI Xin-yu, XIA Wei-jun, YAN Hong-ge, CHEN Ji-hua, SU Bin, SONG Min, LI Zhen-zhen, LU Yang. High strength and large ductility of a fine-grained Al−Mg alloy processed by high strain rate hot rolling and cold rolling [J]. Materials Science and Engineering A, 2020, 787: 139481.
[20] MA K, HU T, YANG H, TOPPING T, YOUSEFIANI A, LAVERNIA E J, SCHOENUNG J M. Coupling of dislocations and precipitates: Impact on the mechanical behavior of ultrafine grained Al−Zn−Mg alloys [J]. Acta Materialia, 2016, 103: 153−164.
[21] DIXIT M, MISHRA R S, SANKARAN K K. Structure−property correlations in Al 7050 and Al 7055 high-strength aluminum alloys [J]. Materials Science and Engineering A, 2008, 478: 163−72.
[22] FAN Cai-he, OU Ling, HU Ze-yi, YANG Jian-jun, CHEN Xi-hong. Re-dissolution and re-precipitation behavior of nano-precipitated phase in Al−Cu−Mg alloy subjected to rapid cold stamping [J]. Transactions of Nonferrous Metals Society of China, 2019, 29(12): 2455−2462.
[23] WANG Wen-guang, WANG Gang, GUO Guan-nan, RONG Yi-ming. Competitive relationship between thermal effect and grain boundary precipitates on the ductility of an as-quenched Al−Cu−Mn alloy [J]. International Journal of Damage Mechanics, 2018, 27(5): 779−2798.

应变速率对喷射成形 Al−Cu−Mg 合金显微组织和力学性能的影响

沈 彤[1]，范才河[1,2]，胡泽艺[1]，吴 琴[1]，倪雨朦[1]，陈昱洲[3]

1. 湖南工业大学 材料与先进制造学院，株洲 412007；
2. 安徽建业科技有限公司，淮北 235000；
3. 湖南智融科技有限公司，株洲 412000

摘 要：采用透射电镜(TEM)、X 射线衍射(XRD)、电子背散射技术(EBSD)和拉伸测试等手段，研究 420 ℃大应变轧制过程中应变速率(0.1、1、9.1 s^{-1})对喷射成形 Al−Cu−Mg 合金显微组织和力学性能的影响。结果表明：在热轧变形过程中，随着应变速率的增大，大角度晶界比例和动态再结晶(DRX)程度先增大后减小，平均晶粒尺寸和位错密度先减小后增大，基体中 S'相数量减少，晶界析出相的粗化及不连续程度增加。当应变速率从 0.1 s^{-1} 增大至 9.1 s^{-1} 时，合金的抗拉强度从 492.45 MPa 下降至 427.63 MPa，伸长率由 12.1%先增加到 21.8%，随后减小到 17.7%。

关键词：喷射成形；Al−Cu−Mg 合金；应变速率；显微组织；力学性能

(Edited by Bing YANG)